ECCOMAS Congress 2016
VII European Congress on Computational Methods in Applied Sciences and Engineering
M. Papadrakakis, V. Papadopoulos, G. Stefanou, V. Plevris (eds.)
Crete Island, Greece, 5–10 June 2016

A MODIFIED SSG/LRR-ω REYNOLDS STRESS MODEL FOR PREDICTING BLUFF BODY AERODYNAMICS

Csaba Klajbár[1], László Könözsy[2], and Karl W. Jenkins[2]

[1]Centre for Fluid Mechanics and Computational Science
Cranfield University, Cranfield, Bedfordshire, MK43 0AL, United Kingdom
e-mail: c.klajbar@cranfield.ac.uk

[2] Centre for Fluid Mechanics and Computational Science
Cranfield University, Cranfield, Bedfordshire, MK43 0AL, United Kingdom
e-mail: laszlo.konozsy@cranfield.ac.uk, k.w.jenkins@cranfield.ac.uk

Keywords: SSG/LRR-ω Reynolds Stress Models, turbulent flow separation, complex vortical structures, computational fluid dynamics (CFD).

Abstract. *This work focuses on a complex turbulent flow around a blunt body by predicting vortical structures, separation/re-attachment locations and velocity/turbulent kinetic energy profiles relying on a modified SSG/LRR-ω Reynolds Stress Model (RSM). The investigated physical problem is in the centre of research interest, because the Reynolds-Averaged Navier-Stokes (RANS) turbulence models and Large Eddy Simulation (LES) approaches usually fail to reproduce the physically correct flow field. Due to the fact that there is lack of knowledge on the SSG/LRR-ω hybrid RSM closure model proposed by Cecora et al. [1], therefore this work has been devoted to further investigate the overall numerical behaviour of a modified hybrid RSM approach. The advantage of these RSM closure models is to take into account the anisotropy of Reynolds stresses caused by the streamline curvature, which has importance in maintaining the quasi non-diffusive nature of turbulent vortices. The numerical model implementation has been verified through the classical test case of a turbulent flow over a flat plate at zero pressure-gradient on a sequence of nested grids. A preliminary analysis performed on this benchmark problem showed that the hybrid model is capable of predicting the near-wall turbulence in the fully-developed boundary layer with a reasonable accuracy. It has also been observed that the SSG/LRR-ω adopts a free-stream independence feature of the specific dissipation rate from the Menters [2] k-ω SST model, thus the turbulent quantities in the near-wall exhibit almost negligible sensitivity respect to the specific dissipation rate outside of the shear layer. In this work, a modified hybrid SSG/LRR-ω RSM closure in conjunction with a simplified diffusion model has been proposed, which has been investigated through the classical cubic obstacle problem in a three-dimensional channel flow of Martinuzzi and Tropea [3]. An increased accuracy and demanding computational time have been observed by employing the modified SSG/LRR-ω formulation, which could still be advantageous, because it unifies the favourable features of two distinct differential Reynolds stress models producing accurate results in the near-wall and the shear layer regions.*

1 INTRODUCTION

Most engineering flows used in aerodynamic design and optimisations for a wide range of applications are almost exclusively turbulent [1, 2, 3]. Therefore several advanced turbulence modelling approaches are proposed over the last twenty years, including advanced scale-resolving techniques as Direct Numerical Simulation (DNS) or Large-Eddy Simulation (LES). The numerical treatment of turbulent flows in general is complicated task and the reliability of numerical tools is always in the centre of interest. The practical applicability of these methods is computationally very demanding, because when the Reynolds number increases, the size of the smallest turbulent structures decreases, thus the computational cost drastically increases. In contrast with that, Reynolds-Averaged Navier-Stokes (RANS) approaches treat turbulent flows by considering the average influence of turbulence on the mean flow by employing classical turbulence models. These engineering turbulence modelling tools are widely used for industrial applications due to their efficiency, robustness and acceptable accuracy, however there are many limitations related to these models caused by the modelling assumptions.

The differential Reynolds stress models (RSMs) are considered as the most advanced RANS tools. This concept originates from the work of Launder et al. [4] and these models completely abandon the Boussinesq-hypothesis, which usually causes the poor performance of the popular eddy-viscosity models. Six transport equations are solved for the Reynolds stresses tensor components and one equation for the turbulent length scale. In these models, the contribution of Reynolds stresses are added directly to the momentum equation instead of employing eddy-viscosity models. The SSG/LRR-ω Reynolds stress model was first proposed by Eisfeild and Brodersen [5]. In addition to the original version of the aforementioned Reynolds stress model, a hybrid SSG/LRR-ω model was developed by Cecora et al. [1] in 2015.

In the present work, the recently developed hybrid SSG/LRR-ω model [1] has been further improved, thus a modified hybrid SSG/LRR-ω approach with a simplified diffusion model has been proposed. The hybrid RSM of Cecora et al. [1] was developed by adopting Menter's blending concept [2], the SSG model of Speziale et al [6] is employed in the near-wall region, and the LRR-ω model of Launder et al. [4] is applied on the rest of the domain. The hybrid RSM closure [1] was primarily developed for aerospace applications, thus its performance for bluff body flows is not yet well-known and it is an interest of the present paper. Therefore the physical problem of an incompressible flow behind a cubic obstacle placed in a three-dimensional channel, which is a classical bluff body test case investigated by Martinuzzi and Tropea [3], has been used to assess the proposed modified hybrid SSG/LRR-ω model.

2 GOVERNING EQUATIONS AND NUMERICAL IMPLEMENTATION

2.1 Reynolds-Averaged Navier-Stokes (RANS) equations

For modelling unsteady, incompressible turbulent flows with Reynolds-Averaged Navier-Stokes (RANS) approach, the governing equations consist of the continuity and momentum conservation laws which can be written [9] with index notation as

$$\frac{\partial \bar{u}_i}{\partial x_i} = 0, \tag{1}$$

$$\frac{\partial}{\partial t}(\rho \bar{u}_i) + \bar{u}_j \frac{\partial}{\partial x_j}(\rho \bar{u}_i) = -\frac{\partial \bar{p}}{\partial x_i} + \frac{\partial}{\partial x_j}\left(2\mu S_{ij} - \rho R_{ij}\right), \tag{2}$$

where $\bar{u}_i$ is the Reynolds-averaged (time-averaged) velocity vector, $\bar{p}$ is the hydrodynamic pressure, ρ is the fluid density, μ is the dynamic viscosity which are considered to be constants. The mean rate of strain tensor S_{ij} represents the averaged viscous stresses of a Newtonian fluid as

$$S_{ij} = \frac{1}{2}\left(\frac{\partial \bar{u}_i}{\partial x_j} + \frac{\partial \bar{u}_j}{\partial x_i}\right). \tag{3}$$

The term ρR_{ij} is the Reynolds stress tensor on the right-hand side of the momentum equation 2, which represents the averaged contribution of turbulence to the mean flow. The elements of this tensor are unknown, thus six additional terms need to be modelled by a suitable closure.

2.2 Differential Reynolds Stress Models

The highest level approximation of the Reynolds stress tensor can be achieved by employing differential Reynolds stress models. In these cases, the eddy-viscosity hypothesis is completely removed from the six transport equations for the components of the Reynolds stress tensor and an additional equation has to be solved for the turbulent length scale which is required for the closure. These RSM models are computationally more expensive, because the solution of the coupled system of partial differential transport equations could lead to numerical instabilities. In addition to this, the unknown terms require modelling assumptions similar to the RANS modelling approaches, which are inevitable sources of uncertainties. Due to these reasons, Reynolds stress models are rarely used for industrial applications, because the general performance of a well-calibrated RANS eddy-viscosity model could also be better. The Reynolds stress transport equations by neglecting the effects of buoyancy and system rotation can be written as

$$\frac{\partial}{\partial t}\left(\rho R_{ij}\right) + \frac{\partial}{\partial x_k}\left(\rho R_{ij}\bar{u}_k\right) = \rho P_{ij} + \rho \Pi_{ij} - \rho \epsilon_{ij} + \rho D_{ij} + \rho M_{ij}, \tag{4}$$

where ρP_{ij} represents the Reynolds stress production, $\rho \Pi_{ij}$ is the pressure-strain correlation tensor, $\rho \epsilon_{ij}$ is the kinetic energy dissipation tensor, ρD_{ij} is the diffusion tensor. It is important to note that the last term is the fluctuating mass flux tensor ρM_{ij} which is neglected for modelling incompressible flows. The elements of the Reynolds stress production tensor are functions of the Reynolds stresses and the derivatives of the mean velocity components as

$$\rho P_{ij} = -\rho R_{ik}\frac{\partial \bar{u}_j}{\partial x_k} - \rho R_{jk}\frac{\partial \bar{u}_i}{\partial x_k}. \tag{5}$$

The reason for neglecting the fluctuating mass flux is that it would represent the contributions of density fluctuations to the Reynolds stress transport equation, which are not present for incompressble flows, thus this term is equal to zero ($\rho M_{ij} = 0$).

2.3 Transport equations of the hybrid SSG/LRR-ω Reynolds Stress model

The SSG/LRR-ω full Reynolds stress model proposed by Cecora et al. [1] is a hybrid combination of Speziale-Sarkar-Gatski (SSG) [6] and Launder-Reece-Rodi (LRR) [4] models by employing Menter's [2] blending concept. The primary motivation for constructing this model was to unify the advantageous features of the aforementioned RSMs. The SSG model formulation is a widely used pressure-strain correlation model, however it employs the turbulent dissipation rate ϵ as a length scale variable. For external aerodynamics, the specific dissipation rate ω was proven to be more advantageous than the application of the dissipation rate ϵ,

therefore the SSG model is used in conjunction with a modified form of Menter's equation for the specific dissipation rate ω in the farfield [2]. The LRR-ω re-distribution model is employed without wall-reflection terms near to the viscous wall. For the hybrid SSG/LRR-ω model proposed by Cecora et al. [1], the pressure-strain correlation tensor is modelled by neglecting the effects of pressure dilation as

$$\begin{aligned}\rho\Pi_{ij} = &-\left(C_1\rho\epsilon + \frac{1}{2}C_1^*\rho P_{kk}\right)a_{ij} + C_2\rho\epsilon\left(a_{ik}a_{kj} - \frac{\delta_{ij}}{3}a_{kl}a_{kl}\right) + \\ &+\left(C_3 - C_3^*\sqrt{a_{kl}a_{kl}}\right)\rho k S_{ij}^* + C_4\rho k\left(a_{ik}S_{jk} + a_{jk}S_{ik} - \frac{2}{3}a_{kl}S_{kl}\delta_{ij}\right) + \\ &+ C_5\rho k\left(a_{ik}W_{jk} + a_{jk}W_{ik}\right),\end{aligned} \tag{6}$$

and the Reynolds stress anisotropy tensor can be computed with the turbulent kinetic energy by

$$a_{ij} = \frac{R_{ij}}{k} - \frac{2}{3}\delta_{ij}, \tag{7}$$

and the mean rate of rotation tensor can be defined as

$$W_{ij} = \frac{1}{2}\left(\frac{\partial\bar{u}_i}{\partial x_j} - \frac{\partial\bar{u}_j}{\partial x_i}\right). \tag{8}$$

The turbulent dissipation rate in the pressure-strain correlation tensor (6) can be expressed by using the specific turbulent dissipation rate ω with a closure constant $C_\mu = 0.09$ as

$$\epsilon = C_\mu k\omega, \tag{9}$$

and the model coefficients in Eq. (6) can be obtained with a blended manner as

$$C_i = F_1 C_i^{(\omega)} + (1 - F_1)C_i^{(\epsilon)}, \quad i = 1, ..., 5; \tag{10}$$

$$C_i^* = (1 - F_1)C_i^{(\epsilon)}, \quad i = 1, 3, \tag{11}$$

where F_1 denotes the blending function, which is similar to that one used in the k-ω SST model proposed by Menter [2]. The model constants used in the present work have been shown in Table 1, which are divided into inner ω and outer ϵ coefficients. The closure parameters were derived from the $C_i^{(\omega)}$ and $C_i^{(\epsilon)}$ constants of the LRR-ω and SSG models, respectively.

The blending function F_1 in Eqs. (10) and (11) ensures that the LRR-ω model acts close to the viscous wall and the SSG formulation is employed on the rest of the computational domain. The function F_1 was developed in a way to be equal to 1 starting from the wall up to approximately 50% of the boundary layer and after that it tends gradually to 0. The blending function depends on global fluid properties, such as dynamic viscosity and fluid density, and on turbulence-related quantities, such as turbulent kinetic energy and specific dissipation rate, and it also takes into account the distance d of the cell to the nearest viscous wall as

$$\begin{aligned}&F_1 = tanh(\zeta^4),\\ &\zeta = min\left[max\left(\frac{\sqrt{k}}{C_\mu\omega d}, \frac{500\mu}{\rho\omega d^2}\right), \frac{4\sigma_\omega^{(\epsilon)}\rho k}{CD_\omega d^2}\right],\\ &CD_\omega = \frac{\sigma_d^\epsilon\rho}{\omega}max\left(\frac{\partial k}{\partial x_k}\frac{\partial\omega}{\partial x_k}, 0\right).\end{aligned} \tag{12}$$

Inner constants: LRR (ω)		Outer constants: SSG (ϵ)	
$\alpha_\omega^{(\omega)} = 0.5556$	$\beta_\omega^{(\omega)} = 0.075$	$\alpha_\omega^{(\epsilon)} = 0.44$	$\omega^{(\epsilon)} = 0.08282$
$\sigma_\omega^{(\omega)} = 0.5$	$\sigma_d^{(\omega)} = 0$	$\sigma_\omega^{(\epsilon)} = 0.856$	$\sigma_d^{(\epsilon)} = 1.712$
$C_1^{(\omega)} = 1.8$	$C_1^{*(\omega)} = 0$	$C_1^{(\epsilon)} = 1.7$	$C_1^{*(\epsilon)} = 0.9$
$C_2^{(\omega)} = 0$	$C_3^{(\omega)} = 0.8$	$C_2^{(\epsilon)} = 1.05$	$C_3^{(\epsilon)} = 0.8$
$C_3^{*(\omega)} = 0$	$C_4^{(\omega)} = \big(9C_2^{(LRR)} + 6\big)/11$	$C_3^{*(\epsilon)} = 0.65$	$C_4^{*(\epsilon)} = 0.625$
$D^{(\omega)} = 0.75C_\mu$	$C_5^{(\omega)} = \big(-7C_2^{(LRR)} + 10\big)/11$	$D^{(\epsilon)} = 0.22$	$C_5^{(\epsilon)} = 0.2$
$C_2^{(LRR)} = 0.52$			

Table 1: Closure coefficients of the SSG/LRR-ω full Reynolds stress model proposed by Cecora et al. [1].

In order to ensure computational robustness and efficiency, the diffusion term is modelled by employing a so-called *simplified diffusion model*, which takes into account the effects of molecular and turbulent diffusion in a simplified way as

$$\rho D_{ij} = \frac{\partial}{\partial x_k}\left[\left(\mu + D_S \frac{\rho k}{C_\mu \omega}\right)\frac{\partial R_{ij}}{\partial x_k}\right], \quad D_S = 0.5C_\mu F_1 + \frac{2}{3}0.22(1 - F_1), \tag{13}$$

and the dissipation term is modelled through an isotropic tensor as

$$\rho\epsilon_{ij} = \frac{2}{3}\rho\epsilon\delta_{ij}, \tag{14}$$

where the turbulent dissipation rate ϵ is predicted by using the specific dissipation rate ω based on Eq. (9). An altered form of Menter's ω-equation is used to supply the length scale where only minor differences were made in the production (ρG_ω), destruction (ρY_ω) and cross-diffusion terms (ρCD_ω) compared to the original ω-equation [2] to adapt to the hybrid model as

$$\begin{aligned}
&\frac{\partial}{\partial t}(\rho\omega) + \frac{\partial}{\partial x_i}(\rho U_i \omega) = \rho G_\omega - \rho Y_\omega + \rho D_\omega + \rho CD_\omega, \\
&\rho G_\omega = \alpha_\omega \frac{\omega}{k}\frac{\rho P_{kk}}{2}, \quad \rho Y_\omega = \beta_\omega \rho \omega^2, \quad \rho D_\omega = \frac{\partial}{\partial x_k}\left[\left(\mu + \sigma_\omega \frac{\rho k}{\omega}\right)\frac{\partial \omega}{\partial x_k}\right], \\
&\rho CD_\omega = \frac{\sigma_d^\omega \rho}{\omega} max\left(\frac{\partial k}{\partial x_k}\frac{\partial \omega}{\partial x_k}, 0\right)
\end{aligned} \tag{15}$$

It is important to note that the cross-diffusion term ρCD_ω makes the link between the k-ϵ and k-ω model behaviours, and Reynolds stress models inherits this term. The closure coefficients are obtained in a blended manner in Eq. (10) with $C_i = \alpha_\omega,\ \beta_\omega,\ \sigma_\omega$ and σ_d, and the model constants of the ω-equation can be found in Table 1.

2.4 Implementation of the modified SSG/LRR-ω model

The modified hybrid SSG/LRR-ω approach with a simplified diffusion model is not available by default in the ANSYS-FLUENT commercial software package [10], therefore according to the best of our knowledge, the present work is one of the first attemps to implement the modified RSM in the ANSYS-FLUENT environment. The modified hybrid SSG/LRR-ω model has been implemented by using User-Defined Functions (UDFs) in C programming language. For the system of governing equations, 6+1 User-Defined Scalar (UDS) transport equations have

been solved by adding the corresponding turbulent source terms to the scalar momentum equations. The incompressible continuity and Reynolds momentum equations were solved by using the pressure-based ANSYS-FLUENT solver [10] through the implemented modified hybrid SSG/LRR-ω model by solving the additional RSM scalar transport equations. The convective flux terms of the momentum equations and the turbulent RSM-UDS transport equations were discretised by using a 2^{nd}-order upwind scheme. In order to ensure convergence to the numerical solutions, all residuals were required to be dropped below a threshold value of 10^{-6}. It was shown by monitoring all shear-stress related quantities that the prescribed criterion was a sufficient condition for ensuring numerical convergence of the solution.

3 RESULTS AND DISCUSSION

The implementation of the modified hybrid SSG/LRR-ω approach with a simplified diffusion model has been compared to the SSG and LRR-ω models on two fundamentally different test cases. The first benchmark problem is a turbulent flow over a flat plate at zero pressure gradient which is an extensively used validation test case for investigating and verifying RANS turbulence model code implementations. The second one is a very challenging flow problem as a turbulent flow past a cube placed in a three-dimensional channel flow which was investigated by Martinuzzi and Tropea [3]. For modelling this physical problem, RANS approaches may fundamentally fail and even LES techniques may also not able to capture accurately the vortical structures of an aerodynamic turbulent flow behind a bluff body at high Reynolds numbers.

3.1 Turbulent flow over a flat plate at zero pressure gradient

The sketch of a fairly simple two-dimensional turbulent flow problem over a flat plate at zero pressure gradient has been shown in Figure 1. The lower boundary starts with an *inviscid* wall section which is followed by a *viscous* wall extending from $x/L = 0.0$ to $x/L = 2.0$, where $L = 1\,m$ is the reference length. The subsonic air enters into the domain at the left velocity inlet boundary at a low Mach number ($Ma = 0.2$). Due to the low magnitude of the farfield Mach number, the fluid flow can be considered as incompressible. The Reynolds number Re_L is defined by the reference length ($Re_L = 5 \cdot 10^6$). By considering these physical circumstances, the maximum boundary layer thickness is estimated as $\delta_{max} \approx 0.03 \cdot L$, thus the domain height of $y/L = 1.0$ can be taken to be high enough to avoid the effect of the upper *inviscid* wall on the near-wall boundary layer flow. The fluid flow leaves the domain at the right *outflow* boundary where the normal derivatives of the velocity components are vanished.

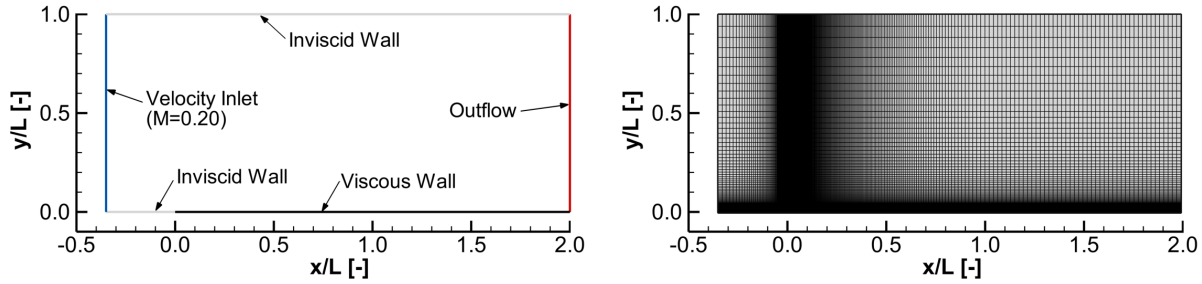

Figure 1: Computational domain with boundary conditions (left) and the computational grid (right) of the flow over a flat plate problem.

A structured computational grid consists of 273×193 node points was used for the com-

putations on the solid plate (see Figure 1). The dimensionless distance y^+_{wall} was kept below 1 in the near wall cells, because the boundary layer was fully-resolved without using any type of wall-function. Furthermore, grid points have been clustered in the direction y and stretched near the leading edge of the plate in order to capture accurately the high gradients of flow variables.

3.1.1 Performance of the modified SSG/LRR-ω model for the flat plate problem

The dimensionless velocity profile u^+ as a function of the dimensionless wall-distance y^+ and the skin friction coefficient c_f distribution along the plate surface have been used to assess the model performance as

$$u^+ = \frac{u}{u_\tau}, \quad y^+ = \frac{u_\tau \cdot y}{\nu}, \quad \text{where} \quad u_\tau = \sqrt{\frac{\tau_w}{\rho}}, \tag{16}$$

and the skin friction coefficient can be written as

$$c_f = \frac{\tau_w}{0.5\rho U^2_\infty A}. \tag{17}$$

The numerical results have been compared to the theoretical curves of Coles [11] and von Kármán & Schroerr [12] (see Figure 2). The worst agreement was produced by the ϵ-based SSG model, because significant discrepancy has been observed in the u^+-y^+ profile outside of the buffer layer while the skin friction c_f distribution was over-predicted. The observed relatively poor performance for predicting near-wall turbulence can be explained with the fact that the SSG model was developed primarily for shear flows. The LRR-ω RSM model performed fairly well for both metrics and an almost perfect match was achieved for the law-of-the-wall and the skin friction coefficient distributions. This property is related to the excellent ability of ω-based models for predicting wall-bounded turbulent flows. The modified SSG/LRR-ω model performed in between the previous two formulations. The tendency of the dimensionless velocity profile was predicted correctly, and above a certain portion of the log-law region, it produced significant discrepancy. The skin friction curve matched well with the theoretical prediction.

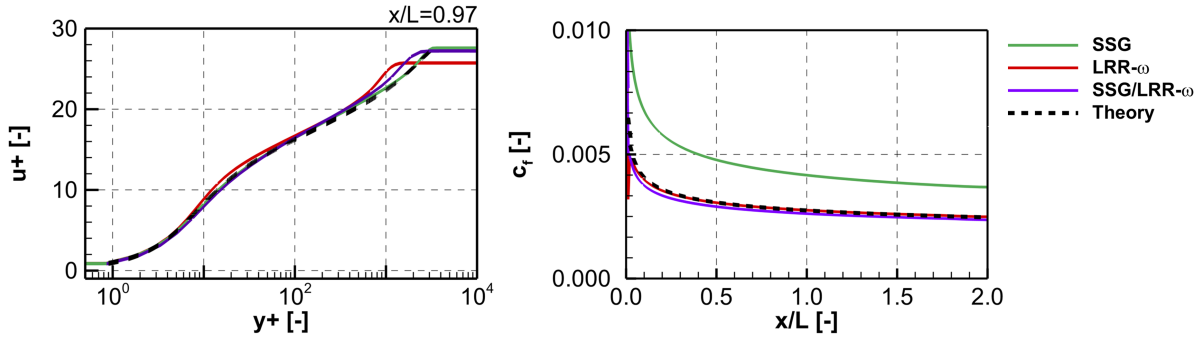

Figure 2: Computed law-of-the-wall compared with the theory of Coles [11] at the $x/L = 0.97$ location (left) and skin-friction coefficient distribution along the wall compared with the von Kármán-Schoenherr [12] theory (right).

3.1.2 Freestream dependency of the specific turbulent dissipation rate ω

There is another important advantage of the SSG/LRR-ω model related to its 7^{th} transport equation. The LRR-ω model employs an altered form of Wilcox's ω-equation [8] for determining the turbulent length scale while the SSG/LRR-ω model was developed with a slightly

modified version of Menter's ω-equation [2]. The k-ω formulation of Wilcox is known to produce freestream dependence of ω which means that the results near the wall strongly depend on the magnitude of the turbulent specific dissipation rate specified outside of the shear layer. This can lead to significant increase in the turbulent viscosity, thus excessive μ_t may prevent flow separation in certain cases. In the development of the k-ω SST model, Menter's [2] one of key motivations was to propose an ω-based turbulence model which has an excellent freestream independence of the k-ϵ formulation. This property is accomplished by adding the so-called cross-diffusion term to the ω-equation, and as a result of that, the predicted near-wall turbulence of the k-ω SST model is far less sensitive to the prescribed ω magnitude at the inlet boundary. This is a very important feature of the this model, because the ω-related boundary conditions are determined relying on differernt assumptions, which are usually sources of uncertainty.

It was observed by relying on numerical experience that although the contribution of ω is obviously different for Reynolds stress models compared to the linear eddy-viscosity models, however the previous properties are inherited in some extent. Numerical investigations have been carried out by using three different ω^{inlet} values of $0.1 \cdot \omega_\infty$, $1 \cdot \omega_\infty$, $10 \cdot \omega_\infty$, where ω_∞ is defined based on the recommendations of Rumsey [13] as

$$\omega_\infty = \frac{3/2(Tu_\infty)^2 \rho U_\infty^2}{\mu_{t,\infty}}, \tag{18}$$

where the farfield turbulence intensity Tu_∞ is taken to be equal to 0.001 and the farfield turbulent viscosity $\mu_{t,\infty}$ is assumed to be equal to 0.1μ. The normalised eddy-viscosity (μ_t/μ) and normalised Reynolds stress (Re^+_{xx}, Re^+_{yy}) distributions can be expressed by

$$\frac{\mu_t}{\mu} = \frac{\rho k}{\omega \mu}, \qquad Re^+_{xx} = \frac{Re_{xx}}{u_\tau} \quad \text{and} \quad Re^+_{yy} = \frac{Re_{yy}}{u_\tau}, \tag{19}$$

which are compared at the $x/L = 0.97$ coordinate with the LRR-ω and the modified SSG/LRR-ω models (see Figure 3). The LRR-ω formulation predicted a clearly higher magniture of μ_t/μ peak over an elongated extent for the lower freestream turbulent dissipation case ($0.1 \cdot \omega_\infty$) compared to the other inlet values. The hybrid RSM exhibited considerably less numerical sensitivity, because very minor deviations can be observed between the corresponding μ_t/μ curves. This is also valid for the normalised Reynolds stress distributions: a) the LRR-ω model predicted approximately 20% increase in the peak mean stress magnitudes for the $\omega^{inlet} = 0.1 \cdot \omega_\infty$, and b) the SSG/LRR-$\omega$ closure produced almost identical Reynolds stress distributions.

3.2 Flow past a cube placed in a three-dimensional channel

The benchmark problem of Martinuzzi and Tropea [3] is a flow past a cubic obstacle placed in a fully-developed turbulent channel flow (see Figure 4). Despite of the fact that the geometry is relatively simple, fairly complex flow structures can be observed around the bluff object. Due to the blockage effect of the body, a strong adverse pressure gradient develops resulting to the formation of the system of horseshoe- and hairpin vortices. Capturing these flow features poses challenges for classical RANS and even advanced scale-resolving turbulence models, thus the investigation of this physical problem can be considered as a long-lasting research topic. In this case, the subsonic inflow is characterized by a bulk Reynolds number ($Re_b = 40\,000$) which is defined by the obstacle height H and bulk average flow velocity U_b. Unsteady simulations have been carried out with a CFL number of 0.95 until the flow time of $50 \cdot H/U_{mean}$ is reached. After that $20 \cdot H/U_{mean}$ time period was used to collect statistical averages of the flow field.

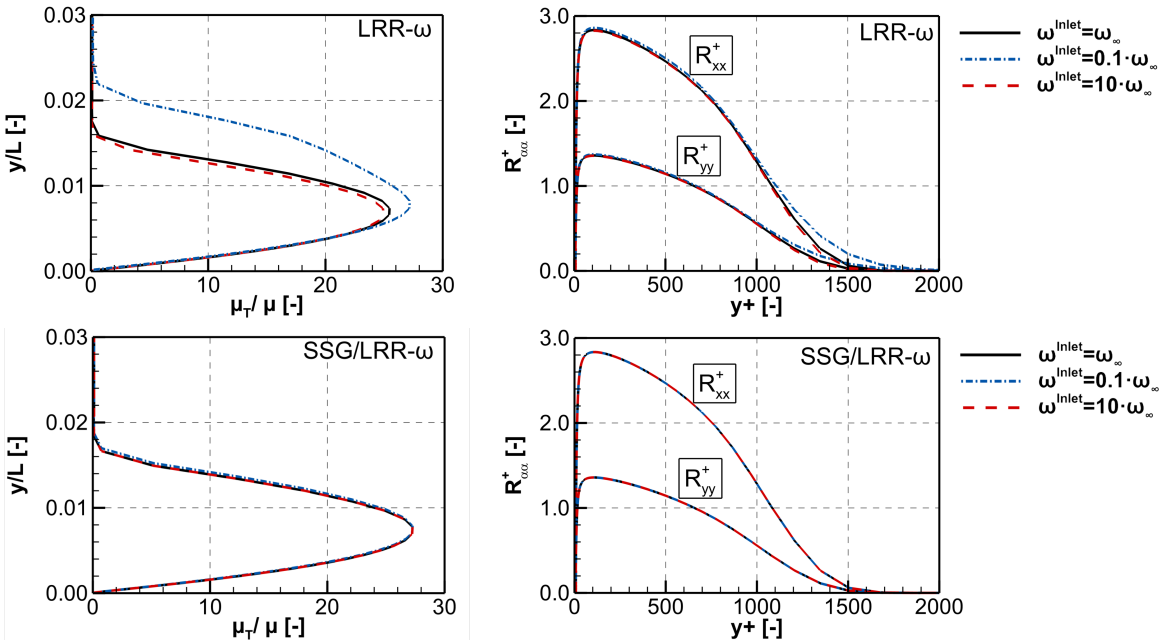

Figure 3: Normalised turbulent viscosity distribution along the vertical direction (left) and normalised Reynolds stress distribution as the function of dimensionless wall distance (right) at the $x/L = 0.97$ location.

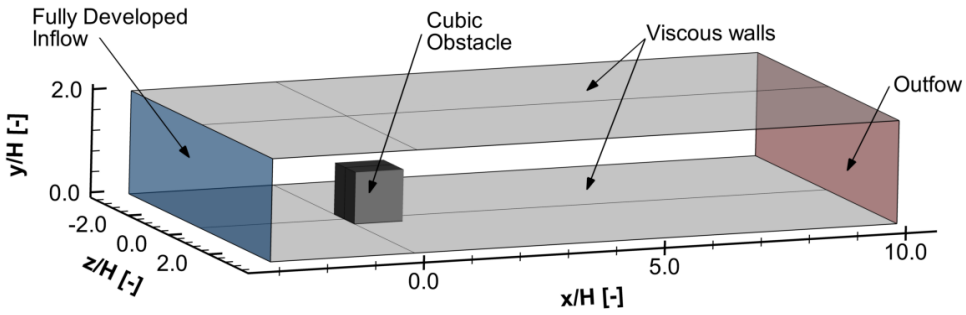

Figure 4: Sketch and boundary conditions of the flow past a cubic obstacle problem.

The boundary conditions of this benchmark problem have been shown in Figure 4. A fully-developed inflow is specified at the inlet plane and the velocity distribution has been obtained through preliminary streamwise periodic channel flow simulations. The cubic obstacle and the upper/lower channel surfaces are treated as viscous walls with no-slip boundary conditions. The two side walls are treated as symmetry planes and the normal derivatives of the velocity compontnes vanish at the outlet section of the channel. A structured computational grid has been employed for the analysis of this benchmark problem (see Figure 5). After performing a grid sensitivity study, the final configuration employs $190 \times 100 \times 120$ cells in directions of x, y and z with the total number of $2\,280\,000$ hexahedral volumes. Near the viscous walls, the grid spacing has been chosen in a way to ensure y^+_{wall} approximately equal to 1.

3.2.1 Performance of the modified SSG/LRR-ω model for a flow past a cube

The numerical results obtained with the aforementioned three turbulence models have been presented in this subsection. The iso-surfaces of Q-criterion indicate that similar upstream

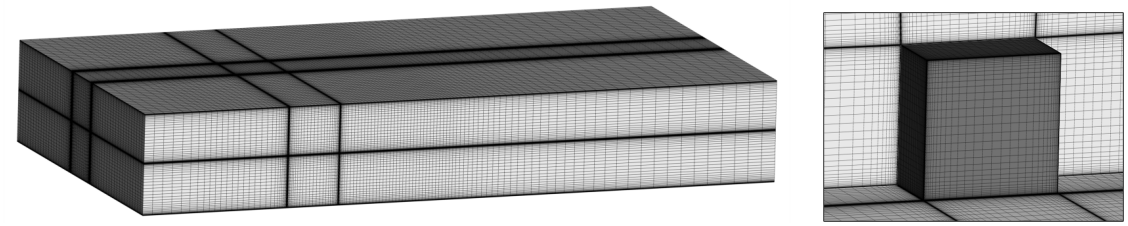

Figure 5: Details of the structured grid prepared for the flow past cube problem.

horseshoe vortex system can be predicted by all models (see Figure 6). However, some remarkable qualitative differences can be observed downstream. In contrast with the SSG closure model, the LRR-ω model was not able to reproduce properly the slanted horseshoe vortex structures behind the cube. The modified SSG/LRR-ω model resulted qualitatively better agreement with the expected vortical flow structures, however the hairpin vortex system on the spanwise faces of the cube were missing and not captured by the SSG model.

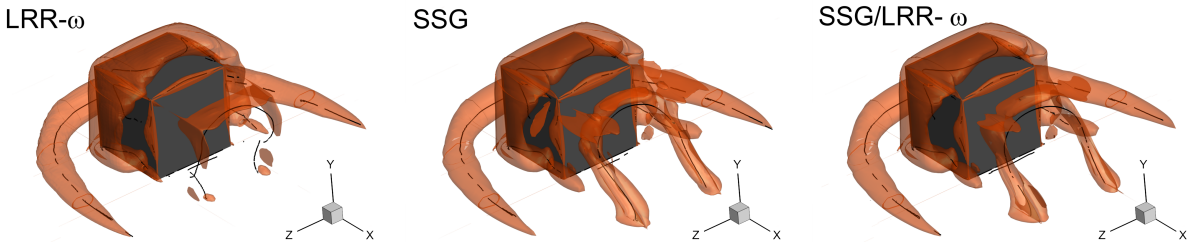

Figure 6: Computed iso-surfaces of Q-criterion for the flow past cubic obstacle problem.

Two mean flow quantities have been compared to the experimental data of Martinuzzi and Tropea [3] (see Table 2). These quantities are the flow separation point upstream and the reattachment location behind the cube in the mid-plane ($z/H = 0$), respectively. In general, all considered models produced remarkable differences for these measures. The separation location was predicted with at least approximately 13% relative error, and the downstream flow quantity was computed with even worse fidelity. These observations confirm again how difficult is to capture such a complex flow around a bluff body.

Configuration	$x_S/H[-]$	$x_R/H[-]$	$\lvert r_S\rvert[\%]$	$\lvert r_R\rvert[\%]$
Experiment	-1.040	2.612	$-$	$-$
SSG	-1.183	3.148	13.75	20.52
LRR-ω	-0.844	3.426	18.85	31.16
SSG/LRR-ω	-1.174	3.207	12.89	22.78

Table 2: Computed flow separation and reattachment locations along the X coordinate direction in the $z/H = 0$ plane, compared with the experimental data of Martinuzzi and Tropea [3].

The normalised streamwise velocity distributions have been compared at the $z/H = 0$ plane at three distinct x coordinates with the experimental data of Martinuzzi and Tropea [3] and the LES solution of Sedighi and Farhadi [14] (see Figure 7). It can be seen that none of the models was particularly successful again. At the $x/H = 0.5$ location, the SSG model slightly

under-predicted the strength of the mean flow above the cube and produced stronger reversed-flow near the cube surface. In contrast with that, the LRR-ω model resulted a stronger mean flow and a weaker recirculatory region. The modified SSG/LRR-ω performed again in between these two approaches indicating the inhereted mixed model properties. At the trailing edge of the cube ($x/H = 1.0$), larger recirculatory zone has been obtained with all RSMs, and it can be seen that even the reference LES simulation produced serious discrepancies. One edge distance downstream of the cube ($x/H = 2.0$), the flow is still massively separated posing serious challenges for all models. Note that the LRR-ω model resulted oscillatory velocity distribution which has not been observed with the SSG and SSG/LRR-ω models. The SSG RSM performed better in terms of agreement with experimental data compared to the hybrid model.

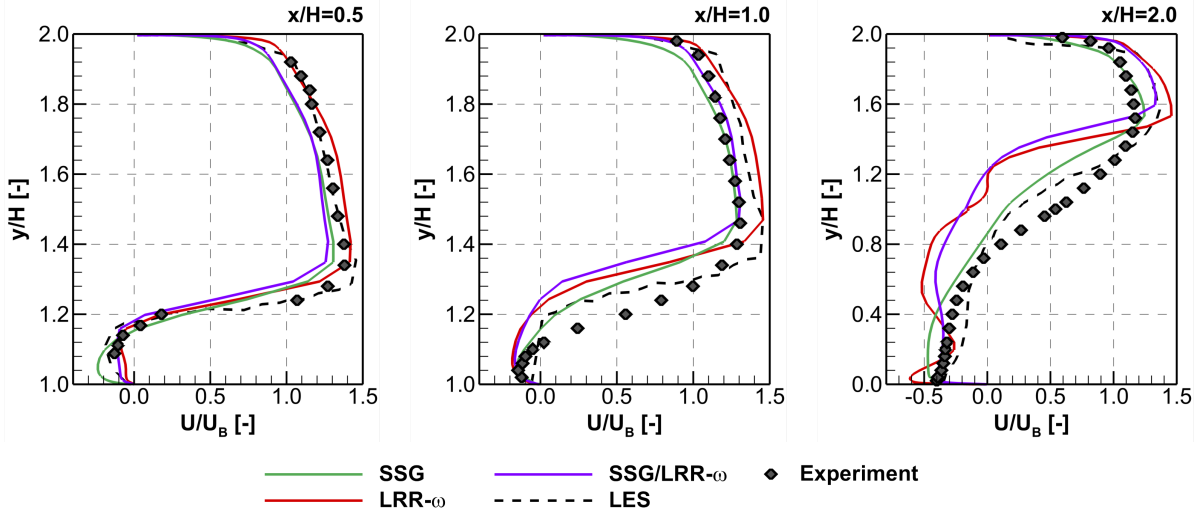

Figure 7: Comparison of normalized streamvise velocity component in the $z/H = 0$ plane with the measured data of Martinuzzi and Tropea [3] and LES solution of Sedighi and Farhadi [14].

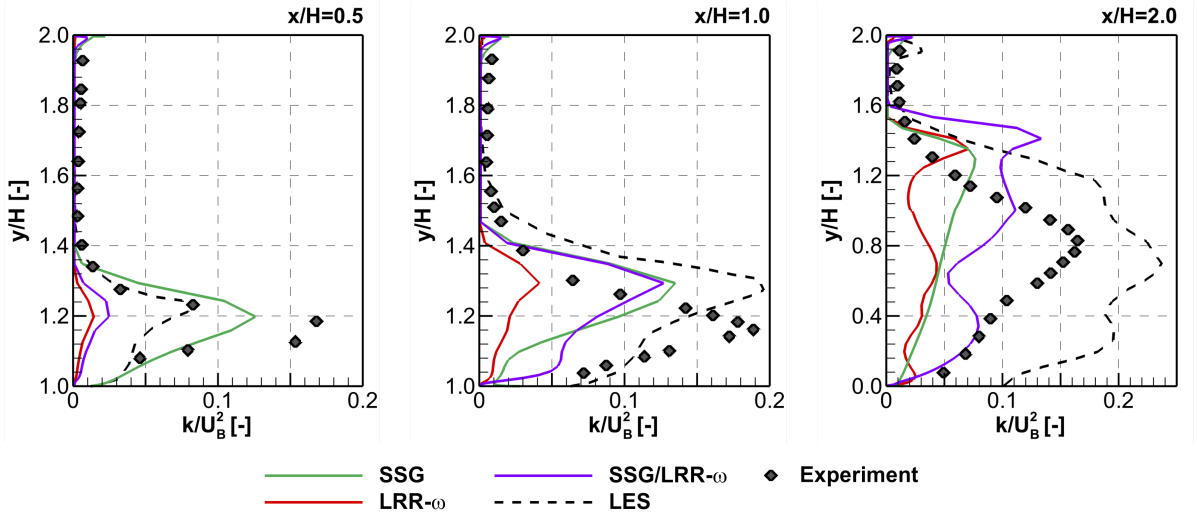

Figure 8: Comparison of normalized turbulent kinetic energy in the $z/H = 0$ plane with the measured data of Martinuzzi and Tropea [3] and LES solution of Sedighi and Farhadi [14].

The normalised turbulent kinetic energy distribution have been investigated along the previously shown locations (see Figure 8). In general, all Reynolds stress models under-predicted the peak magnitudes which indicates that the investigated RSMs produced excessive dissipation of the turbulent flow structures. This dissipative behaviour was the most striking for the LRR-ω model and the less drastic for the SSG model. The hybrid closure RSM performed in between these aforementioned two RSMs. It is important to note again that large errors have been obtained against the LES results of Sedighi and Farhadi [14].

4 CONCLUSIONS

In this work, a modified hybrid SSG/LRR-ω RSM approach with a simplified diffusion model has been investigated through the classical cubic obstacle problem in a three-dimensional channel flow of Martinuzzi and Tropea [3]. This model is blending the advantageous features of two distinct RSMs: a) the LRR-ω model, which is used to compute simple wall bounded flows, and b) the SSG model, which was developed for shear flows. Preliminary performance analysis on the problem of a flow over a flat plate at zero pressure gradient showed that the proposed RSM was able to reproduce law-of-the-wall accurately. It was also observed that the hybrid closure provides the freestream independence of the specific turbulent dissipation rate ω, which means that the results at near the wall was not sensitive to the ω quantity specified outside of the shear layer. In addition to this, the modified hybrid SSG/LRR-ω model has been assessed for the classical bluff body problem of a flow past cube in a three-dimensional channel flow. It was observed that the accuracy of the investigated RSM model was in between the obtained results of the LRR-ω and SSG approaches to predict a complex vortical flow around a bluff body. Since the original version of the hybrid SSG/LRR-ω model proposed by Cecora et al. [1] was primarily developed for aeronautical applications, therefore further improvements for bluff body aerodynamics are still required. The numerical results indicate that existing RANS models should also be further improved for capturing the aforementioned complex flow structures, furthermore it can be seen that LES techniques, which requires orders of magnitude higher computational effort, are challenged to predict these flows accurately. Overall, it can be concluded that the modified hybrid SSG/LRR-ω RSM approach with a simplified diffusion model exhibited stable numerical behaviour for computing a complex flow around a bluff body.

REFERENCES

[1] Cecora, R.-D., Radespiel, R., Eisfeld, B., Probst, A., Differential Reynolds Stress Modeling for Aeronautics. *AIAA Journal*, **53**(3), 739–755, 2015.

[2] Menter, F. R., Two-Equation Eddy-Viscosity Turbulence Models for Engineering Applications. *AIAA Journal*, **32**(8), 1598–1605, 1994.

[3] Martinuzzi, R., Tropea, C., The flow around surface-mounted prismatic obstacles placed in a fully developed channel flow. *Journal of Fluids Engineering*, **115**, 85–91, 1993.

[4] Launder, B. E., Reece, G. J., Rodi, W., Progress in the development of a Reynolds-stress turbulence closure. *Journal of Fluid Mechanics*, **68**, Part 3, 537–566, 1975.

[5] Eisfeild, B., Brodersen, O., Advanced Turbulence Modelling and Stress Analysis for the DLR-F6 Configuration. *AIAA Paper* 2005–4727, 2005.

[6] Speziale, C. G., Sarkar, S., Gatski, T. B., Modelling Modelling the Pressure-Strain Correlation of Turbulence - An Invariant Dynamical Systems Approach. *NASA Contractor Report 181979*, *ICASE Report*, **90-5**, 1990.

[7] Gibson, M. M., Launder, B. E., Ground Effects on Pressure Fluctuations in the Atmospheric Boundary Layer. *Journal of Fluid Mechanics*, **86**, 491–511, 1978.

[8] Wilcox, D. C., Re-assessment of the scale-determining equation for advanced turbulence models. *AIAA Journal*, **26**(11), 1299–1310, 1988.

[9] Wilcox, D. C., *Turbulence Modeling for CFD, 2nd Edition*. DCW Industries, La Canada, 1998.

[10] ANSYS Inc., ANSYS FLUENT Theory Guide. *ANSYS*, Release 14.0, November, 2011.

[11] Coles, D. J., Fluid Mechanics. *RAND Corp. Report*, **R-403-PR**, 191–226, 1962.

[12] von Kármán, Th., Turbulence and Skin Friction. *Journal of the Aeronautical Sciences*, **1**(1), 1–20, 1934.

[13] Rumsey, C. L., Turbulence Modelling Resource. *NASA, Langley Research Center*, Available online: http://turbmodels.larc.nasa.gov/, cited on 20^{th} of February 2016.

[14] Sedighi, K., Farhadi, M., Three-Dimensional Study of Vortical Structure Around a Cubic Bluff Body in a Channel. *Facta Universitas, Mechanical Engineering*, **4**(1), 1–16, 2006.